ACS APPLIED MATERIALS & INTERFACES

www.acsami.org

Research Article

Stability, Elastic Properties, and the Li Transport Mechanism of the Protonated and Fluorinated Antiperovskite Lithium Conductors

Mohammed B. Effat, Jiapeng Liu, Ziheng Lu, Ting Hei Wan, Antonino Curcio, and Francesco Ciucci*

Cite This: *ACS Appl. Mater. Interfaces* 2020, 12, 55011−55022

Read Online

ACCESS | Metrics & More | Article Recommendations | Supporting Information

ABSTRACT: Lithium-rich antiperovskites (APs) have attracted significant research attention due to their ionic conductivity above 1 mS cm^{-1} at room temperature. However, recent experimental reports suggest that proton-free lithium-rich APs, such as Li_3OCl, may not be synthesized using conventional methods. While Li_2OHCl has a lower conductivity of about 0.1 mS cm^{-1} at 100 °C, its partially fluorinated counterpart, $Li_2(OH)_{0.9}F_{0.1}Cl$, is a significantly better ionic conductor. In this article, using density functional theory simulations, we show that it is easier to synthesize Li_2OHCl and two of its fluorinated variants, i.e., $Li_2(OH)_{0.9}F_{0.1}Cl$ and $Li_2OHF_{0.1}Cl_{0.9}$, than Li_3OCl. The transport properties and electrochemical windows of Li_2OHCl and the fluorinated variants are also studied. The *ab initio* molecular dynamics simulations suggest that the greater conductivity of $Li_2(OH)_{0.9}F_{0.1}Cl$ is due to structural distortion of the lattice and correspondingly faster OH reorientation dynamics. Partially fluorinating the Cl site to obtain $Li_2OHF_{0.1}Cl_{0.9}$ leads to an even greater ionic conductivity without impacting the electrochemical window and synthesizability of the materials. This study motivates further research on the correlation between local structure distortion, OH dynamics, and increased Li mobility. Furthermore, it introduces $Li_2OHF_{0.1}Cl_{0.9}$ as a novel Li conductor.

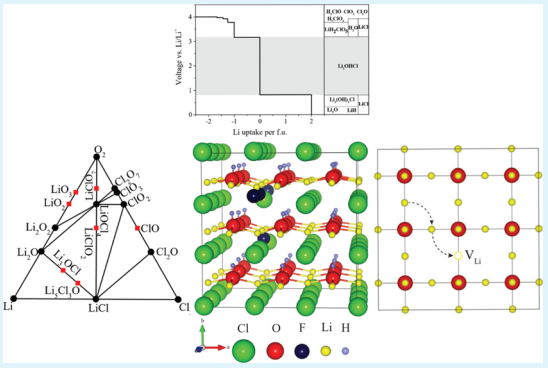

KEYWORDS: *Li_2OHCl, antiperovskite, fluorination, solid-state electrolyte, batteries*

1. INTRODUCTION

The increasing need for enhancing the safety of lithium-ion batteries (LIBs) has triggered many research studies in the area of inorganic solid-state electrolytes (SSEs).[1−3] In fact, unlike their liquid organic counterparts,[4,5] inorganic SSEs are nonflammable and, therefore, intrinsically safer. Several families of inorganic SSEs have been proposed, including the Li-rich antiperovskites (AP).[6,7] Among APs, Li_3OCl has attracted considerable attention because of its high ionic conductivity of >1 mS cm^{-1} at room temperature (RT).[8−11] However, in recent years, various research groups have reported that the synthesis of H-free Li_3OCl is extremely challenging because of its highly hygroscopic nature.[12−16] This lead to a renewed interest in Li_2OHCl, a protonated AP, which is closely related to Li_3OCl.[17]

Hanghofer et al.[14] and Dawson et al.[12] synthesized Li_3OCl and Li_2OHCl. While for Li_3OCl, both research groups reported the formation of significant amounts of secondary phases, including $Li_4(OH)_3Cl$ (31 wt %) and LiCl (9 wt %), "an almost" pure phase of Li_2OHCl was obtained. Although Dawson et al.[12] did not detect impurities in Li_2OHCl, the material made by Hanghofer et al. had <10 wt % of LiCl.[14] In another work, Song and co-workers[13] synthesized Li_2OHCl and observed an impurity of LiCl if the material was heated above 60 °C. Wang et al.[16] synthesized Li_2OHCl and found a LiCl impurity (5 wt %). These studies suggest that it is easier to synthesize Li_2OHCl than Li_3OCl, and also shed light on the phase instability of Li_2OHCl. Since these experimental observations are relatively recent, there are no theoretical investigations dedicated to the study of the synthesizability and phase stability of Li_2OHCl.

The limited ionic conductivity of Li_2OHCl (i.e., ~4.3×10^{-5} and ~0.1 mS cm^{-1} at RT and 100 °C, respectively) is a major challenge.[12,13,17] To unravel the ionic conduction mechanism of Li_2OHCl, Schwering et al.,[18] Song et al.,[13,19] and Dawson et al.[12] used nuclear magnetic resonance and found that the diffusion of Li is correlated with the reorientation of the OH groups. For the orthorhombic phase of Li_2OHCl, which occurs below 30 °C, the OH groups are static and electrostatically block the migration of Li. Instead, in the cubic phase, the H atom of each OH group reorients around the O atom, improving the mobility of Li. To increase the ionic conductivity of Li_2OHCl, Li et al.[15] investigated the impact

Received: October 7, 2020
Accepted: November 17, 2020
Published: November 27, 2020

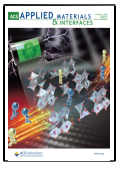

of partial fluorination on the dynamics of the OH sublattice of Li_2OHCl. In particular, these authors synthesized $Li_2(OH)_{1-x}F_xCl$ and found that for $x = 0.1$, the cubic phase is stable at RT. Furthermore, the ionic conductivity was measured to be 0.035 and 1.9 mS cm^{-1} at RT and 100 °C, respectively. Li et al.[15] attributed the enhanced ionic conductivity (relative to Li_2OHCl) to the lower concentration of OH groups. As outlined above, such groups hinder the Li hops Coulombically. However, these authors also discovered that by further decreasing the concentration of OH groups, the ionic conductivity decreased. Yin et al.[20] studied $Li_2OHBr_{1-x}F_x$, a closely related material, experimentally. These researchers found that at RT, the conductivity increased from 0.7×10^{-3} for $x = 0$ to 1.1×10^{-3} mS cm^{-1} for $x = 0.02$. At a higher x, the conductivity dropped. Yin et al.[20] ascribed the improved conductivity to the structural distortion due to the difference in the ionic radius between F and Br. It must be noted that the concentration of OH groups in $Li_2OHBr_{0.98}F_{0.02}$ is the same as that in Li_2OHBr. It is, therefore, natural to pose the following question: is reducing the OH concentration in Li_2OHCl, as done by Li et al.,[15] the only way that allows the ionic conductivity of Li_2OHCl to be improved? In response to this query, it can be argued that altering the Cl sublattice of Li_2OHCl to obtain $Li_2OHCl_{1-x}F_x$ may also lead to faster ionic transport. To test this hypothesis, the ionic conduction mechanism in both $Li_2(OH)_{0.9}F_{0.1}Cl$, the material made by Li et al.,[15] and $Li_2OHF_{0.1}Cl_{0.9}$, a new material we proposed, was studied computationally. We chose to substitute only 10% of Cl with F, i.e., $x = 0.1$ in $Li_2OHCl_{1-x}F_x$, to ensure consistency with the F-substitution level of the paper of Li et al.[15] Incidentally, it should be stressed that there is another gap in the literature: to date, there are no theoretical studies that investigate the impact of fluorination on the Li hopping and OH dynamics of Li_2OHCl.

One should also note that the electrochemical stability of Li_2OHCl and $Li_2(OH)_{0.9}F_{0.1}Cl$ has not been studied. Only two experimental papers have been published on this topic, and there are no computational investigations.[15,17] Moreover, there are neither experimental nor computational studies on the elastic properties of Li_2OHCl and $Li_2(OH)_{0.9}F_{0.1}Cl$ (e.g., Young's modulus, Pugh ratio, etc.). One should note that the hydroscopic nature of the AP electrolytes makes the measurement of the elastic moduli challenging.[21] Thus, theoretical predictions of the elastic moduli are needed. To address all points outlined above, using density functional theory (DFT) and *ab initio* molecular dynamics (AIMD) simulations, the phase and electrochemical stability, the elastic properties, and the ionic conductivity of Li_2OHCl, $Li_2(OH)_{0.9}F_{0.1}Cl$, and $Li_2OHF_{0.1}Cl_{0.9}$ were studied.

Regarding the synthesizability of Li_2OHCl vs Li_3OCl, simulations suggest that Li_2OHCl, $Li_2(OH)_{0.9}F_{0.1}Cl$, and $Li_2OHF_{0.1}Cl_{0.9}$ are easier to make than Li_3OCl, in agreement with the experimental literature.[12−15] In terms of phase stability, Li_2OHCl and its fluorinated variants are found to be metastable at 0 K with energies above hull below 20 meV/atom. As for the electrochemical stability, the electrochemical window of Li_2OHCl and its fluorinated variants is computed to be about 2.3 V vs Li/Li^+, a value much smaller than the experimental value of 9 V vs Li/Li^+ reported by Li et al.[15] for $Li_2(OH)_{0.9}F_{0.1}Cl$. It is also found that the elastic moduli are sensitive to protonation, with the value of Young's modulus computed for Li_2OHCl and Li_3OCl being 43.2 vs 103.0 GPa, respectively. Fluorination also impacts Young's modulus, which is 33.1 GPa for $Li_2OHF_{0.1}Cl_{0.9}$ and 43.1 GPa for $Li_2(OH)_{0.9}F_{0.1}Cl$. Interestingly, the ionic conductivity of $Li_2OHF_{0.1}Cl_{0.9}$ was calculated to be higher than that of $Li_2(OH)_{0.9}F_{0.1}Cl$ (i.e., 0.38 vs 0.05 mS cm^{-1} at RT). From the analysis of the AIMD trajectories, the increase in ionic conductivity was correlated to local structural distortions, brought by fluorination, in the anionic sublattices. In particular, it is found that the mobility of Li increased near the F atoms. It is also noted that the time scale characteristic of OH reorientation in the fluorinated compounds is shorter than that in Li_2OHCl, suggesting a three-way correlation between the structural distortion, the faster OH dynamics, and the increased Li mobility.

Our study enriches the Li_2OHCl-related literature by (1) examining the phase stability of Li_2OHCl and its fluorinated variants; (2) reporting the elastic properties of Li_2OHCl-based electrolytes; (3) showing that fluorination increases the ionic conductivity locally by structural distortion and enhanced OH dynamics; and (4) predicting $Li_2OHF_{0.1}Cl_{0.9}$ as a promising SSE.

2. COMPUTATIONAL METHODS

All DFT computations were performed using the Vienna *ab initio* simulation package (VASP).[22,23] The Perdew−Burke−Ernzerhof (PBE) generalized gradient approximation (GGA) was used as the exchange−correlation functional in all of the calculations except for the computation of the elastic properties and band gaps.[24] Due to their higher accuracy, the PBE functional revised for solids (PBEsol)[25] and the Heyd−Scuseria−Ernzerhof (HSE06)[26] hybrid functional were used for computing the elastic properties and the band gap, respectively. The pymatgen package[27] was used for the analyses of phase stability, electrochemical stability, and the calculations of the reaction energies.

2.1. Structural Optimization. For each nominal composition studied, i.e., Li_2OHCl, $Li_2(OH)_{0.9}F_{0.1}Cl$, and $Li_2OHF_{0.1}Cl_{0.9}$, we first searched for the lowest energy arrangements over 20 000 randomly created structures, see Section S1 of the Supporting Information (SI) for details. The database of the Materials Project with default settings was used as a starting point for the compositional and electrochemical stability analyses.[27−29] Specifically, all structural degrees of freedom including shapes, volumes, and ions' positions were allowed to relax. A 0.05 meV/atom energy convergence criterion was used to obtain the ground-state energy, E_{GS}. The Brillouin zone was sampled on an automatically generated Monkhorst−Pack k-point grid for the cubic phase of the APs, and on a Γ-centered grid for the orthorhombic phase of Li_2OHCl, with a minimum grid density of 1000 per reciprocal atom.[30] All calculations were spin polarized. The energy cutoff, E_{cut}, was set to 520 eV.

2.2. Formation of Electrolytes from Their Precursors. The reaction energy, ΔE, associated with obtaining Li_3OCl, Li_2OHCl, $Li_2(OH)_{0.9}F_{0.1}Cl$, and $Li_2OHF_{0.1}Cl_{0.9}$ was computed from the precursors used experimentally. ΔE is defined as the ground-state energy difference between the products and reactants. $\Delta E < 0$ indicates that the reaction is thermodynamically favorable.

2.3. Phase Stability. The compositional stability of Li_2OHCl was assessed by comparing its normalized ground-state energy, $\overline{E} = E_{GS}/N_{atoms}$ (N_{atoms} is the number of atoms in the material), to that of all phases in the Li−H−O−Cl compositional space.[27,31,32] The phase diagrams were constructed by computing the convex hull for all available phases. The stable compositions are located on the hull, while unstable compositions lie above it, with an energy above the hull, $E_{hull} > 0$. A similar procedure was used to evaluate the phase stability of $Li_2(OH)_{0.9}F_{0.1}Cl$ and $Li_2OHF_{0.1}Cl_{0.9}$ in the Li−H−O−Cl−F compositional space.

2.4. Electrochemical Stability. The electrochemical stabilities of the APs were assessed using two approaches. First, the band gap of each AP was estimated using the HSE06 hybrid functional.[26] It should

https://dx.doi.org/10.1021/acsami.0c17975
ACS Appl. Mater. Interfaces 2020, 12, 55011−55022

be noted that this approach provides an upper limit to the electrochemical window.[33,34] Second, the grand potential phase diagram (GPPD) was used to approximate the electrochemical window.[32,35] The electrolyte is taken to be an open system to Li and it is possible to compute the equilibrium phases formed at the electrode/electrolyte interface for different values of the Li chemical potentials, μ_{Li}. The electrochemical stability window is the range of μ_{Li} within which the electrolyte is neither oxidized nor reduced.[32] The corresponding voltage window can be obtained by taking

$$V = \frac{\mu_{Li}^0 - \mu_{Li}}{e} \quad (1)$$

where μ_{Li}^0 is a reference value for μ_{Li} and e is the elementary charge.

2.5. Elastic Properties. The bulk (B) shear (G) and Young (E) moduli of Li_2OHCl, $Li_2(OH)_{0.9}F_{0.1}Cl$, $Li_2OHF_{0.1}Cl_{0.9}$, and Li_3OCl were calculated using settings identical to those used in the study of other APs.[36] Specifically, E_{cut} and the energy convergence criterion were set at 520 and 10^{-6} eV, respectively, and the structures were relaxed, using the PBEsol functional,[25] until the residual forces on each atom were less than 0.01 eV $Å^{-1}$. Displacement of 0.015 Å was used for the computation of the elastic tensor. From the elastic tensor, the elastic moduli were estimated following the Voigt−Reuss−Hill (VRH) approximation,[36] see Section S2 of the SI.

2.6. *Ab initio* Molecular Dynamics. The AIMD computations were performed for Li_2OHCl, $Li_2(OH)_{0.9}F_{0.1}Cl$, and $Li_2OHF_{0.1}Cl_{0.9}$ at 800, 900, 1000, 1100, and 1200 K. The simulations were carried out in the NVT ensemble with the Nosé−Hoover thermostat to maintain the desired temperature. For all simulations, E_{cut} was set to 400 eV and the energy convergence criterion was set to 10^{-4} eV. The Brillouin zone was sampled at the Γ-point. The total simulation time was 40 ps with a time step of 1 fs. The first 10 ps of the simulation time were treated as an equilibration period. Only the last 30 ps of the simulation were employed for the analysis. The simulations were initialized with the experimental lattice parameters, see Section 3.1.

The mean-square displacement (MSD) of the Li ions was estimated from[37]

$$\mathrm{MSD}_{Li}(t) = \frac{1}{N}\sum_{i=1}^{N} |r_i(t + t_0) - r_i(t_0)|^2 \quad (2)$$

where $r_i(t)$ is the position of the ion i, with i = 1, 2, ...N (N = number of Li atoms in the simulation box) at time t ($t \in [10,40]$ ps) and t_0 = 10 ps. The self-diffusion coefficient, D_{Li}, was estimated using[38]

$$D_{Li} = \frac{\mathrm{MSD}_{Li}}{6t} = D_{Li}^0 \exp\left(-\frac{E_{act}}{k_B T}\right) \quad (3)$$

where D_{Li}^0 is a constant, k_B is Boltzmann's constant, T is the simulation temperature in K, and E_{act} is the activation energy. The temperature-dependent ionic conductivity, $\sigma_{Li}(T)$, was estimated from the Nernst−Einstein relation as[39]

$$\sigma_{Li}(T) = \frac{(z_{Li}e)^2 N D_{Li}}{V k_B T} \quad (4)$$

where z_{Li} is the integer charge of a Li ion (z_{Li} = 1) and V is the volume of the simulation box.

To estimate D_{Li} and σ_{Li}, the last 30 ps of the simulation period were divided into three 10 ps subintervals. Then, the MSD of each of those subintervals was regressed to obtain D_{Li} and σ_{Li}. The average values of σ_{Li} were used to estimate E_{act}. E_{act} and the predicted value of σ_{Li} at 100 °C were estimated by Gaussian process (GP) regression[40,41] of $\log_{10}(\sigma_{Li}T)$ vs $1/T$. The GP regression was performed using a linear mean function and a squared exponential kernel, with evidence-optimized kernel parameters, as implemented in MATLAB.

To gain insight into the diffusion mechanism, the AIMD trajectories were analyzed. The analysis allowed the identification of the Li jumps, as well as the time scale of the OH reorientations. Details about the method are given in Section S3 of the SI. Using the pymatgen diffusion package,[27] the Li occupation maps were generated by binning the ions' positions to their nearest crystallographic sites. The pair radial distribution function was calculated using the visual molecular dynamics (VMD) package.[42]

3. RESULTS AND DISCUSSION

3.1. Ground-State Structures. The ground-state structures of Li_2OHCl, $Li_2(OH)_{0.9}F_{0.1}Cl$, and $Li_2OHF_{0.1}Cl_{0.9}$ and their corresponding energies were obtained following the procedure outlined in Section 2.1 and Section S1 of the SI. The unit cell of the cubic phase of Li_2OHCl ($Pm\bar{3}m$) is shown in Figure 1a. In the cell, $a = b = c$ = 3.91 Å, 1/3 of the Li sites

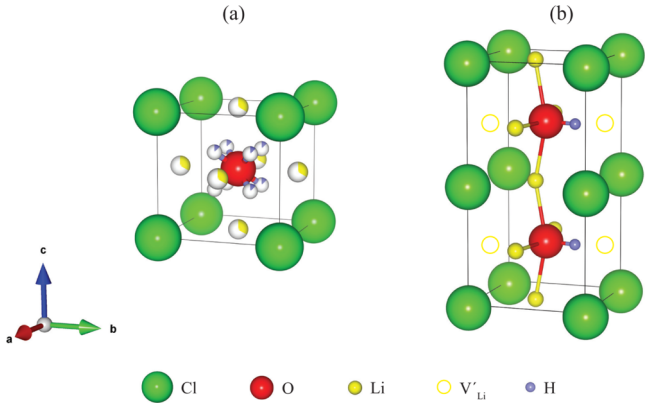

Figure 1. Structure of Li_2OHCl: (a) unrelaxed unit cell model and a (b) relaxed 1 × 1 × 2 supercell.

are vacant, and the OH group point toward Cl. A relaxed 1 × 1 × 2 supercell of Li_2OHCl is shown for reference in Figure 1b. The relaxed structure is tetragonal with $a = c > b$ and characterized by a slight distortion (see Table S2 in the SI). The OH groups are ordered, aligned along the b axis, and point toward the vacant Li sites. This result is consistent with the literature, as the ordering of the OH groups and their alignment toward the shortest lattice parameter were also observed by Howard et al.[43] and Dawson et al.[12] The relaxed structures of $Li_2(OH)_{0.9}F_{0.1}Cl$ and $Li_2OHF_{0.1}Cl_{0.9}$ are pseudocubic, see Table S3 and Figure S2. The OH groups are characterized by a similar alignment as Li_2OHCl.

3.2. Formation of Li_3OCl, Li_2OHCl, and Fluorinated Electrolytes. It should be noted that both Li_3OCl and Li_2OHCl were synthesized from LiCl and LiOH according to the following equations[8,17]

$$LiCl + 2LiOH \rightarrow Li_3OCl + H_2O \quad (5a)$$

$$LiCl + LiOH \rightarrow Li_2OHCl \quad (5b)$$

The computed ΔEs of eq 5a and 5b were 150 and 4 meV/atom (normalization is based on the number of atoms in Li_3OCL or Li_2OHCl), respectively. While both values are positive, the significantly smaller ΔE of eq 5b compared to eq 5a suggests that it is easier to synthesize Li_2OHCl compared to Li_3OCl.

We mentioned in the introduction that several research groups were able to synthesize an almost pure phase of Li_2OHCl but found the synthesis of H-free Li_3OCl to be challenging.[12,14,17,18] To illustrate this point, Dawson et al.[12] proposed that Li_3OCl could take up H_2O, giving Li_2OHCl according to the equation

https://dx.doi.org/10.1021/acsami.0c17975
ACS Appl. Mater. Interfaces 2020, 12, 55011−55022

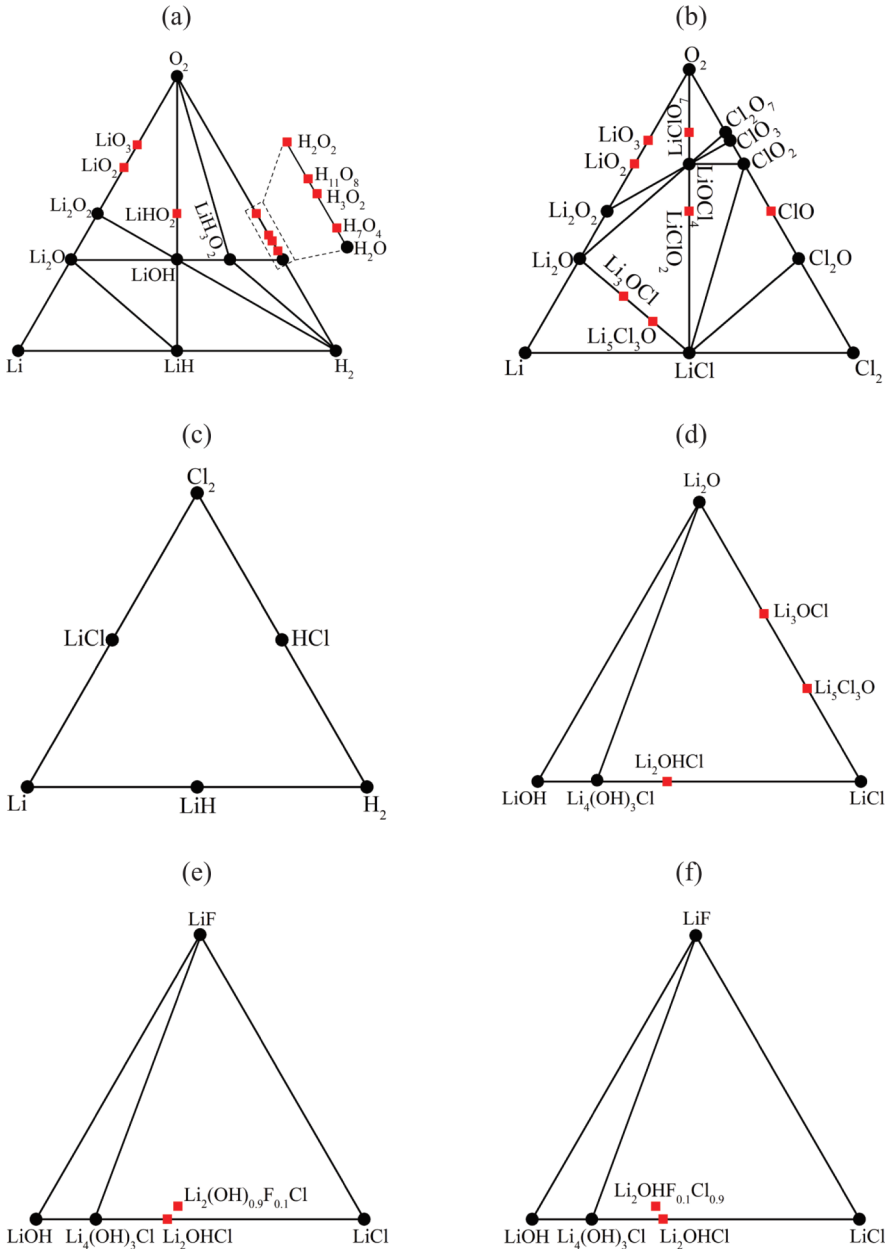

Figure 2. Projections of the compositional phase diagrams of (a–d) Li_2OHCl, (e) $Li_2(OH)_{0.9}F_{0.1}Cl$, and (f) $Li_2OHF_{0.1}Cl_{0.9}$. (a–d) Li–O_2–H_2, Li–O_2–Cl_2, Li–H_2–Cl_2, and Li_2O–LiOH–LiCl Gibbs triangles of Li_2OHCl, respectively. (e, f) LiOH–LiCl–LiF Gibbs triangles of $Li_2(OH)_{0.9}F_{0.1}Cl$ and $Li_2OHF_{0.1}Cl_{0.9}$, respectively. The black dots represent stable phases. The red squares indicate unstable phases.

$$Li_3OCl + \frac{1}{2}H_2O \rightarrow Li_2OHCl + \frac{1}{2}Li_2O \quad (6)$$

Dawson et al.[12] reported ΔE of eq 6 to be −0.148 meV/atom. We calculated ΔE of eq 6 to be = −0.09 meV/atom, where the negative ΔE underlines the hygroscopic nature of Li_3OCl. It should be pointed out that the slight difference in ΔE is likely due to the different exchange–correlation functionals used in each study, i.e., PBE in this study vs PBEsol used by Dawson et al.[12] Furthermore, Hanghofer et al.[14] found $Li_4(OH)_3CL$ and LiCl impurities in their synthesized sample of Li_3OCl. Following this evidence, we calculated ΔE of the following reaction

$$Li_3OCl + H_2O \rightarrow \frac{2}{3}Li_4(OH)_3Cl + \frac{1}{3}LiCl \quad (7)$$

The computed ΔE was −0.173 meV/atom, a value more negative than that of eq 6. This value further supports the experimental evidence that obtaining Li_3OCl is challenging. Given the negative ΔEs of eqs 6 and 7, the synthesis of Li_2OHCl appears to be "easier" compared to that of Li_3OCl.

Regarding the fluorinated APs, Li et al.[15] made $Li_2(OH)_{0.9}F_{0.1}Cl$ from LiF, LiOH, and LiCl. Consequently, ΔE of these two reactions can be computed

$$LiF + 8LiOH + 9LiCl \rightarrow Li_{18}(OH)_8Cl_9F \quad (8a)$$

$$LiF + 9LiOH + 8LiCl \rightarrow Li_{18}(OH)_9Cl_8F \quad (8b)$$

The ΔEs were 10.4 and 7.8 meV/atom (normalization is based on the number of atoms in $Li_{18}(OH)_8Cl_9F$ and $Li_{18}(OH)_9Cl_8F$) for eq 8a and 8b, respectively. These ΔEs are comparable to that of eq 5b and are smaller than that of eq

https://dx.doi.org/10.1021/acsami.0c17975
ACS Appl. Mater. Interfaces 2020, 12, 55011–55022

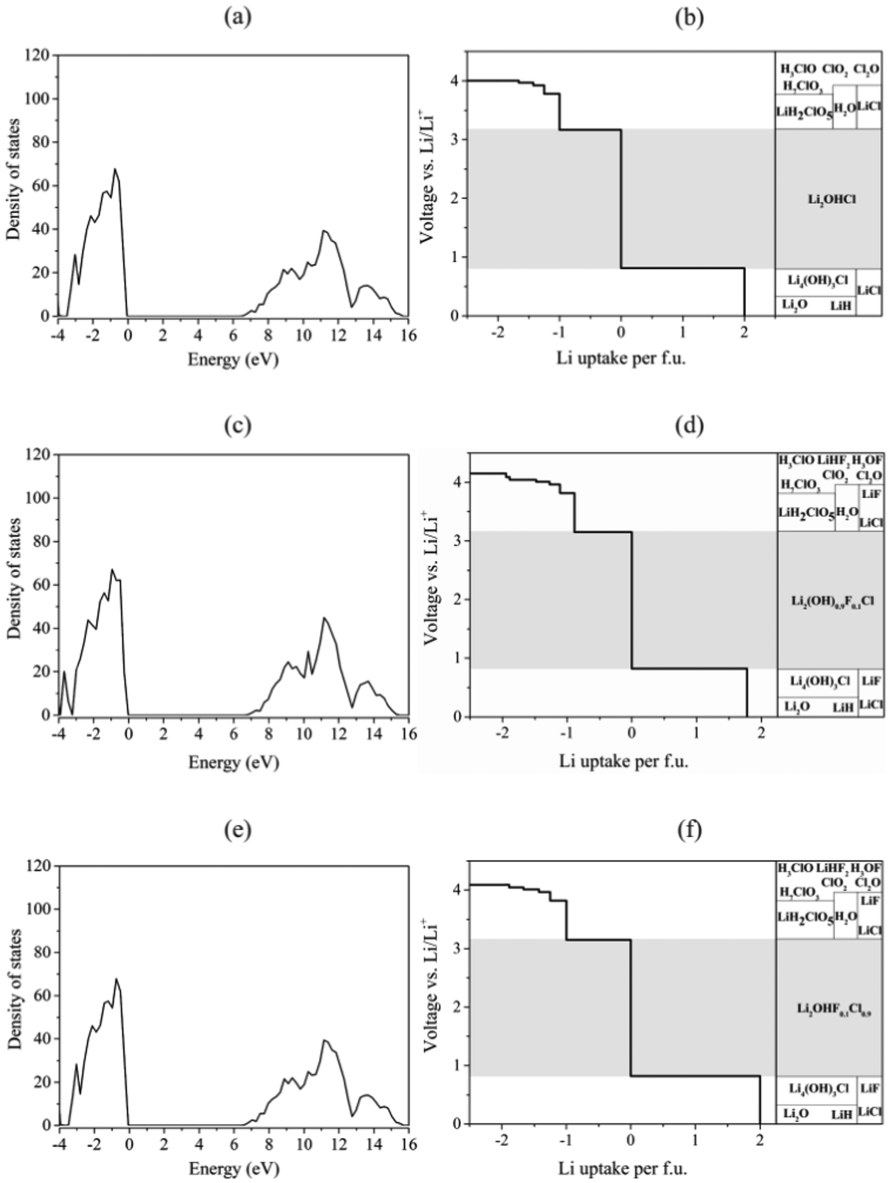

Figure 3. Electrochemical stability windows of (a, b) Li_2OHCl, (c, d) $Li_2(OH)_{0.9}F_{0.1}Cl$, and (e, f) $Li_2OHF_{0.1}Cl_{0.9}$. Band gap, left-hand panels, and GPPD, right-hand panels, with computed phases as a function of voltage vs Li/Li^+.

5a. Interestingly, we note that ΔE of $Li_2OHF_{0.1}Cl_{0.9}$ eq 8b is smaller than that of $Li_2(OH)_{0.9}F_{0.1}Cl$ eq 8a.

3.3. Phase Stability. *3.3.1. Li_2OHCl.* The phase stability of Li_2OHCl was assessed by constructing its phase diagram. As viewing the Li−O−H−Cl Gibbs tetrahedron is unfeasible on the paper, Figure 2a−c reports the Li−O_2−H_2, Li−O_2−Cl_2, and Li−Cl_2−H_2 projections. Figure 2d shows the Li_2O−LiOH−LiCl Gibbs triangle, whose corner compositions are those of the precursors used in the synthesis of Li_2OHCl. In all phase diagrams, the black dots and red squares represent stable and unstable phases, respectively.

As illustrated in Figure 2d, Li_2OHCl is predicted to be unstable, with Li_2OHCl decomposing into LiCl and $Li_4(OH)_3Cl$, see eq 9. E_{hull} was calculated to be 11 meV/atom

$$Li_2OHCl \rightarrow \frac{2}{3}LiCl + \frac{1}{3}Li_4(OH)_3Cl \quad (9)$$

We mentioned in the introduction that Hanghofer et al.,[14] Song et al.,[13] and Wang et al.[16] detected impurities of LiCl in the Li_2OHCl samples but did not find $Li_4(OH)_3Cl$. One possible explanation for this experimental observation is that the energetic barrier that needs to be overcome for the formation of LiCl (a binary compound) is lower than the one required for $Li_4(OH)_3Cl$ (a quaternary compound).[44] Hanghofer et al.[14] reported that the X-ray diffraction (XRD) spectra of Li_2OHCl (*Pban*) have two reflections at 36.8 and 49.5° that can be assigned to $LiCl{\cdot}xH_2O$ (x = 1−6).[45] When refining synchrotron XRD and neutron powder diffraction spectra of the orthorhombic phase of Li_2ODCl, Wang et al.[16] found reflections that could not be assigned to specific phases. We quote from that article: "three phases excluding the LiCl impurity appear better suited to fit the data (Figure S4), but the exact nature of these individual phases cannot be determined conclusively".

Therefore, both experimental observations and our DFT predictions suggest that Li_2OHCl is metastable, likely decomposing into LiCl and other impurities, which may include $Li_4(OH)_3Cl$. However, for a precise examination of the

https://dx.doi.org/10.1021/acsami.0c17975
ACS Appl. Mater. Interfaces 2020, 12, 55011−55022

phase stability, this computational study needs to be accompanied by dedicated experiments to identify the precise nature of such impurities.

3.3.2. Fluorinated Li_2OHCl. The phase diagrams of $Li_2(OH)_{0.9}F_{0.1}Cl$ and $Li_2OHF_{0.1}Cl_{0.9}$ are shown in Figure 2e,f, respectively. Both APs are predicted to be unstable with E_{hull} = 17 and 15 meV/atom, respectively. The decomposition products are predicted to be LiF, LiCl, and $Li_4(OH)_3Cl$ following

$$Li_2(OH)_{8/9}F_{1/9}Cl \rightarrow \frac{1}{9}LiF + \frac{19}{27}LiCl + \frac{8}{27}Li_4(OH)_3Cl \quad (10a)$$

$$Li_2OHF_{1/9}Cl_{8/9} \rightarrow \frac{1}{9}LiF + \frac{5}{9}LiCl + \frac{3}{9}Li_4(OH)_3Cl \quad (10b)$$

While there is no experimental evidence yet that these impurities are also generated during the synthesis of $Li_2(OH)_{0.9}F_{0.1}Cl$, it is noted that E_{hull} of both $Li_2(OH)_{0.9}F_{0.1}Cl$ and $Li_2OHF_{0.1}Cl_{0.9}$ is small (<20 meV/atom) and close to that of Li_2OHCl (11 meV/atom). Consequently, entropy[46] may stabilize the two APs, giving "almost pure" phases.

3.4. Electrochemical Stability. *3.4.1. Li_2OHCl.* The electron density of states and the voltage of Li_2OHCl and its fluorinated variants vs Li uptake per formula unit (fu) are shown in Figure 3, left-hand and right-hand panels, respectively. The band gap of Li_2OHCl, shown in panel (a), implies that the electrochemical window is ~6.6 V. On the other hand, thermodynamic predictions from GPPD, see Figure 3b, show that Li_2OHCl is reduced below 0.82 V and oxidized above 3.15 V vs Li/Li^+. These two voltages suggest that the electrochemical window is limited to ~2.3 V. Unless the decomposition products formed in the first few cycles between the electrolyte and battery electrodes have a higher electrochemical window than the one computed, and form a protective solid electrolyte interphase layer (SEI), the operational voltage windows of Li_2OHCl-based batteries will be limited.[47,48] The full decomposition reactions between Li and Li_2OHCl and the corresponding voltages are listed in Table S4 in the SI.

There are no available experimental data on the electrochemical window of Li_2OHCl. Hood et al.[17] cycled 160 times a symmetric Li-metal cell with Li_2OHCl as the electrolyte. By analyzing the Li_2OHCl | Li-metal interface with energy-dispersive X-ray spectroscopy, these researchers detected Li_2O and LiCl in the SEI, suggesting that the following reaction took place

$$Li_2OHCl + Li \rightarrow Li_2O + LiCl + \frac{1}{2}H_2 \quad (11)$$

At 0 V, see Figure 3b, the following decomposition reaction was predicted:

$$Li_2OHCl + 2Li \rightarrow Li_2O + LiCl + LiH \quad (12)$$

which is in agreement with eq 11, except for the evolution of H_2. However, according to Hood et al.,[17] H_2 might evolve from the interface and SEI likely contained unreacted lithium metal, as the interfacial reaction between the Li and Li_2OHCl is self-limiting. In turn, Li and H_2 might react as follows[49]

$$Li + \frac{1}{2}H_2 \rightarrow LiH \quad (13)$$

where ΔE is −0.48 eV/atom, in agreement with eq 11.

It is notable that Li_2O and LiCl are reported to be beneficial constituents of the SEI layer formed between Li and Li_2OHCl because they can prevent the further decomposition of the electrolyte.[17] For instance, the reduction and oxidation limits of LiCl are 0 and 4 V vs Li/Li^+, respectively.[50] Note that at potentials above 3.15 V, various non-Li-containing compounds, such as H_7ClO_3, H_3ClO, ClO_2, and Cl_2O are predicted to form.[51] Because of their low ionic conductivities, these compounds likely deteriorate the battery performance.[52] These results indicate that it is important to protect Li_2OHCl from oxidative decomposition. As explained by Zhu et al.,[50] one strategy is to apply a protective Li-conductive coating, e.g., $LiLa(PO_3)_4$, on the positive electrode.[53]

3.4.2. Fluorinated Li_2OHCl. The band gap and voltage of $Li_2(OH)_{0.9}F_{0.1}Cl$ vs Li uptake are shown in Figure 3c,d, respectively. Panels (e) and (f) of Figure 3 show analogous results for $Li_2OHF_{0.1}Cl_{0.9}$. Tables S5 and S6 list the decomposition reactions and corresponding voltages for $Li_2(OH)_{0.9}F_{0.1}Cl$ and $Li_2OHF_{0.1}Cl_{0.9}$, respectively. By comparing the panels (a) and (b) with (c) and (f) of Figure 3, it is noted that both the band gap and the voltage of the fluorinated APs vs Li uptake are similar to those computed for Li_2OHCl. For instance, for both fluorinated APs, the reduction and oxidation potentials are ~0.82 and 3.15 V vs Li/Li^+, respectively, limiting the electrochemical window to ~2.3 V. Below 0.82 V, LiF is predicted to form.[52] The formation of LiF, which has 0 and 6 V vs Li/Li^+ reduction and oxidation potentials, respectively, might help to protect the lithium metal surface.[54] Above 3.15 V, compounds that are not beneficial to battery performance (i.e., ClO_2, H_7ClO_3, etc.) are expected to materialize. These results again highlight the need for protective coatings on the positive electrode to prevent oxidative decomposition.

The experimental electrochemical window of $Li_2(OH)_{0.9}F_{0.1}Cl$ has been measured using cyclic voltammetry (CV) by Li et al.,[15] who found the oxidation potential to be ~9 V vs Li/Li^+. This value is much higher than predicted 3.15 V. We note that, in a typical CV experiment used to estimate the electrochemical window, the SSE is attached to a planar working electrode (e.g., a disk of stainless steel) and to a Li foil, which acts as a reference and a counter electrode. One substantial drawback of this testing configuration is that the contact between SSE and the working electrode is low. Consequently, the measured current from the CV experiment may be insignificant and therefore hardly detectable, leading to an overestimation of the electrochemical window.[55] Further, as reported in Tables S5 and S6, decomposition reactions include H-containing compounds like LiH_2ClO_5 and H_7ClO_3, and the kinetic barrier to form such compounds may be high. To identify the electrochemical window of Li_2OHCl-based electrolytes more accurately, CV experiments, where SSE is mixed with carbon to make a working electrode are recommended, as doing so extends the accessible area by decomposition reactions.[56,57]

3.5. Elastic Properties. The mechanical properties of SSEs can significantly impact the cycling performance of SSBs.[58−60] Unlike liquid electrolytes that can penetrate through active particles of electrodes, the contact between the SSE and electrode particles is that of a solid with another solid. Therefore, SSEs have to be able to accommodate elastically the volumetric expansion of electrode particles during battery cycling.[61,62] In addition, the assembly and stacking of SSB is

https://dx.doi.org/10.1021/acsami.0c17975
ACS Appl. Mater. Interfaces 2020, 12, 55011−55022

easier if the SSEs are ductile.[63] In light of these two factors, we calculated the moduli B, G, and E, see Table 1.

Table 1. Elastic Moduli and Pugh Ratios of Li_3OCl, Li_2OHCl, $Li_2(OH)_{0.9}F_{0.1}Cl$, and $Li_2OHF_{0.1}Cl_{0.9}$ AP

electrolyte	B bulk modulus (GPa)	G shear modulus (GPa)	E Young's modulus (GPa)	G/B Pugh ratio
Li_3OCl	57.2	42.9	103	0.75
Li_3OCl [ref 36]	55.7	41.5	99.7	0.74
Li_2OHCl	27.6	17.4	43.1	0.63
$Li_2(OH)_{0.9}F_{0.1}Cl$	26.1	17.6	43.2	0.67
$Li_2OHF_{0.1}Cl_{0.9}$	20.2	13.5	33.1	0.67

The predicted values of Li_3OCl are in close agreement with those reported by Deng et al.[36] (see Table 1). The elastic moduli of the protonated and fluorinated variants of Li_3OCl are smaller than that of Li_3OCl, suggesting that Li_2OHCl-based APs are better able to accommodate chemomechanical strain originating from the expansion of the electrodes. Furthermore, the lower stiffness of Li_2OHCl-based APs is likely linked to the lower concentration of Li, consistent with previous reports.[61,64] To check whether the APs are ductile or brittle, the Pugh ratio, G/B, was used as an indicator. According to the literature,[36,65] $G/B = 0.6$ is the limiting value between ductility ($G/B < 0.6$) and brittleness ($G/B > 0.6$). As indicated in Table 1, the Pugh ratio of all electrolytes is >0.6, suggesting that they are brittle. Among them, Li_3OCl has the highest Pugh ratio, while Li_2OHCl has the smallest one. Doping Li_2OHCl with F slightly increases the Pugh ratio. This is expected from chemical intuition and supported by Bader charge analysis[66] (see Section S5 in the SI) that shows that fluorination slightly increases the ionic character of the bonds.

3.6. Ionic Conductivity and Diffusion Mechanism.

3.6.1. Conductivity and Activation Energy. AIMD simulations were performed on the cubic phase of Li_2OHCl-based APs at temperatures ranging from 800 to 1200 K. The GP regression of $\log_{10}(\sigma_{Li}T)$ vs $1/T$ for the three APs studied is shown in Figure 4, together with the estimated activation energies. GP was used to predict the ionic conductivities and compare simulations and experiments, see Table 2.

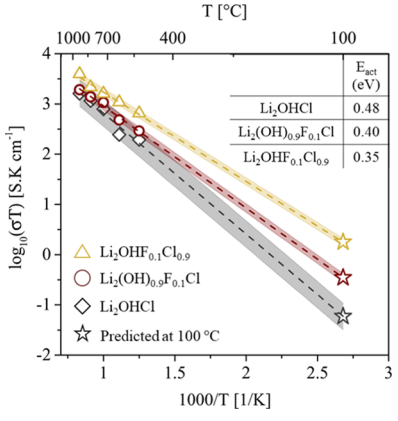

Figure 4. Gaussian process regression of $\log_{10}(\sigma_{Li}T)$ vs $1/T$ to estimate E_{act} and σ_{Li} (100 °C) for Li_2OHCl, $Li_2(OH)_{0.9}F_{0.1}Cl$, and $Li_2OHF_{0.1}Cl_{0.9}$. The dashed lines indicate mean values, while the shaded zones are the 95% credible intervals.

As shown in Table 2, the predictions for Li_2OHCl and $Li_2(OH)_{0.9}F_{0.1}Cl$ are in reasonable agreement with experiments. Interestingly, it can be noted that the predicted conductivity of $Li_2OHF_{0.1}Cl_{0.9}$ is significantly higher than that of Li_2OHCl and $Li_2(OH)_{0.9}F_{0.1}Cl$. Moreover, among all compositions, $Li_2OHF_{0.1}Cl_{0.9}$ has the lowest activation energy for Li migration. This suggests that partial fluorination of the Cl sublattice of Li_2OHCl is an effective method for increasing the ionic conductivity. It is also noted from the MSD plots (at 1100 K), see Figure S4a–c, that Li is the only mobile species in the three studied APs. The occupation maps of Li ions, see Figure S4d–e, show that diffusion of Li appears to be mediated by vacancies in all studied APs.

3.6.2. Diffusion Mechanism. To understand how fluorinating the OH or Cl sublattice of Li_2OHCl impacts the dynamics of Li and OH, the Li and OH trajectories of the AIMD simulations were analyzed. For details regarding the analysis, the reader is invited to consult Section 3 of the SI. The results presented in this subsection were obtained for 1100 K. Results for other temperatures are reported in Section S6.2 of the SI.

The number of Li hops for the three APs is shown in Figure 5a. The fluorinated APs are characterized by higher Li mobility than Li_2OHCl. Regarding the mechanism of diffusion, it is found that it occurs by both individual and concurrent hops, see Section S3 of the SI. The two types of jump are illustrated in Figure 5c,d on a two-dimensional (2D) projection of the Li_3OCl lattice. The solid arrow indicates an individual hop, where an ion directly jumps to an available vacant site. The dashed arrows show a concurrent event, where a Li ion occupies a Li site only after that site is vacated. Individual and concurrent events are shown in Figure 5e,f, respectively.

The analysis suggests that, for the three composition studies, the hops are mainly individual, but the percentage of concurrent hops increases if the APs are fluorinated. The first point is intuitive as Li_2OHCl-based Aps are Li-vacancy rich. The number of Li ions, n, that hopped individually was calculated. As shown in Figure 5b, most of these jumps are due to single Li ions ($n = 1$). Only a few of these events occur as hops of two ions ($n = 2$), see Figure 5e, implying that a fraction (~7%) of the vacant Li sites is occupied. $Li_2OHF_{0.1}Cl_{0.9}$ has the highest number of concurrent events and conductivity among the three studied APs.

As already highlighted in the introduction, the diffusion of Li ions has been correlated to the dynamics of OH reorientation.[12,13,18,19] We investigated whether this holds true for the fluorinated electrolytes $Li_2(OH)_{0.9}F_{0.1}Cl$ and $Li_2OHF_{0.1}Cl_{0.9}$ as well. To that end, we estimated the characteristic time scales of second-order angular autocorrelation function defined as

$$C_2(t) = \langle \rho(P_2[u(0).\, u(t)]) \rangle \tag{14}$$

where ρ is the autocorrelation function,[67] P_2 is the second-order Legendre's polynomial, and $\boldsymbol{u}(0)$ and $\boldsymbol{u}(t)$ are the unit vectors taking the position of an O atom as an origin and pointing toward the H atom. More details are given in Section S3.3 of the SI. The angular autocorrelation functions of Li_2OHCl, $Li_2(OH)_{0.9}F_{0.1}Cl$, and $Li_2OHF_{0.1}Cl_{0.9}$ at 1100 K are shown in Figure 6a–c, respectively. It is noted that there are two time scales. The first time scale (see the insets) is ascribed to the libration of the OH groups.[19,68] The second and slower time scale is associated with reorientations. It should be noted that such a slower time scale has been recently suggested to be correlated to the OH reorientation.[19,68] The longer exponen-

https://dx.doi.org/10.1021/acsami.0c17975
ACS Appl. Mater. Interfaces 2020, 12, 55011–55022

Table 2. Comparison between Experimental and Predicted Values of the Activation Energies and Li Conductivities at 25 and 100 °C

	E_{act} (eV)		$\sigma_{100\ °C}$ (mS cm^{-1})		$\sigma_{25\ °C}$ (mS cm^{-1})	
composition	exp.	comp.	exp.	comp.	exp.	comp.
Li_2OHCl	0.56 [ref 17]	0.48	0.1 [ref 17]	0.16 ± 0.10	not cubic at RT	
$Li_2(OH)_{0.9}F_{0.1}Cl$	0.52 [ref 15]	0.40	1.90 [ref 15]	0.94 ± 0.19	0.04 [ref 15]	0.05 ± 0.01
$Li_2OHF_{0.1}Cl_{0.9}$	N/A	0.35	N/A	4.78 ± 0.84	N/A	0.38 ± 0.08

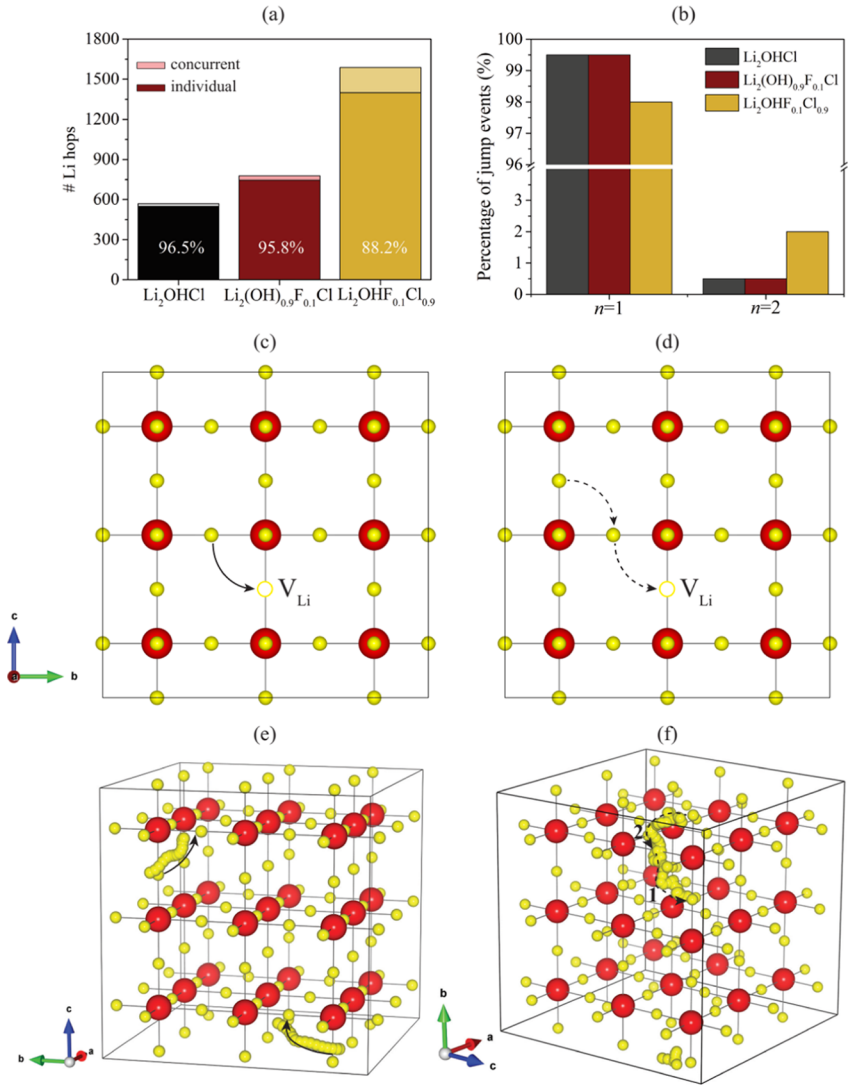

Figure 5. (a) Total number of Li hops for each composition studied. Dark and light-colored portions of the columns represent individual and concurrent hops, respectively. (b) Percentage of individual events occurring as hops of one (n = 1) or two (n = 2) ions. (c, d) 2D schematics illustrating independent and concurrent hops, respectively. (e, f) Representative visualization of individual and concurrent hops.

tial of $C_2(t)$ was fitted to obtain the associated slower time constant. All computed time scales are reported in Tables S8 and S9. The analysis indicates that the time scales of OH reorientations in the fluorinated electrolytes are shorter than that in Li_2OHCl, suggesting a correlation between the faster rotation of the OH groups and the higher conductivity.

We also examined whether fluorination locally increases the Li mobility. For this reason, we counted the number of hops occurring at each Li site in the three studied APs, see Sections S3.2 of the SI, and visualized them in Figure 6d–f. The positions of the circles correspond to the Li sites, with their size scaling linearly with the total number of hops. The locations of F atoms are marked by black stars. By comparing Figure 6d, Li_2OHCl, and Figure 6f, $Li_2OHF_{0.1}Cl_{0.9}$, it is understood that near the F atoms of $Li_2OHF_{0.1}Cl_{0.9}$, Li is more mobile. For $Li_2(OH)_{0.9}F_{0.1}Cl$, as shown in Figure 6e, this phenomenon is less obvious.

The increased Li mobility (and shorter reorientation time scales) of the fluorinated electrolytes is likely due to local structural distortions induced by fluorination. Specifically, the mismatch of the ions' sizes between F, OH, and Cl (1.33, 1.37, and 1.81 Å, respectively)[69] induces distortions that widen the Li-diffusion channels nearby F atoms. As the ionic radius of Cl is bigger than OH, the local structural distortion is more

https://dx.doi.org/10.1021/acsami.0c17975
ACS Appl. Mater. Interfaces 2020, 12, 55011−55022

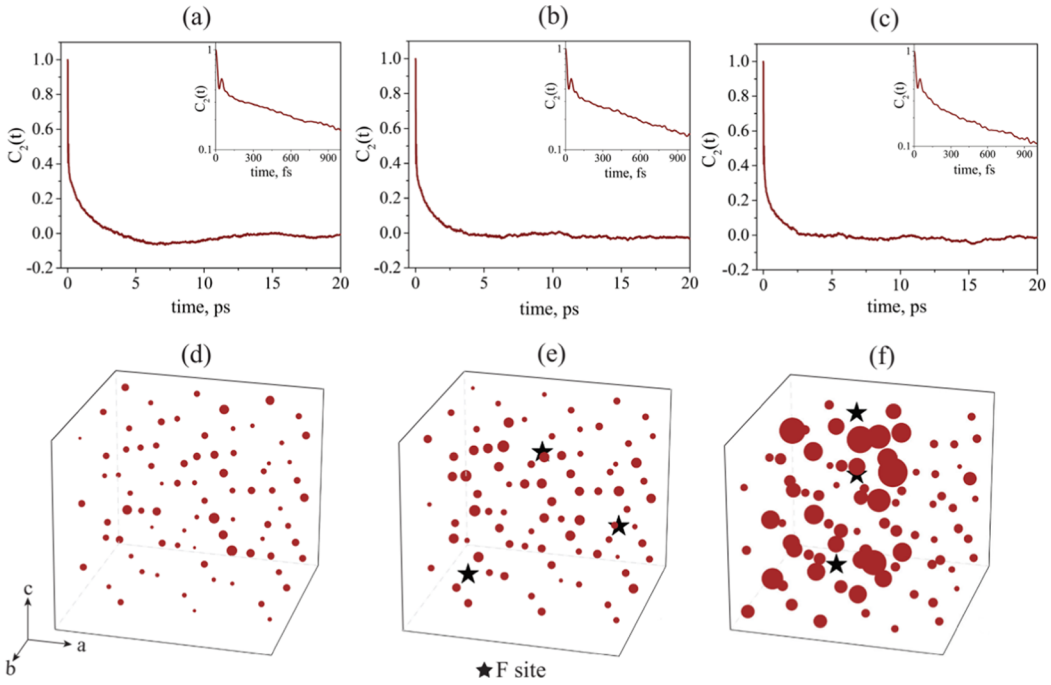

Figure 6. Impact of fluorination on the conductivity of the Li_2OHCl-based APs. Columns from left to right show Li_2OHCl, $Li_2(OH)_{0.9}F_{0.1}Cl$, and $Li_2OHF_{0.1}Cl_{0.9}$. (a, b, c) Second-order angular autocorrelation functions. (d, e, f) Scatter plots visualizing the local mobility of Li in the structures of the APs. Li and F sites are shown by the circles and the black stars, respectively. The size of the circles scales linearly with the total number of Li hops.

significant in $Li_2OHF_{0.1}Cl_{0.9}$ than in $Li_2(OH)_{0.9}F_{0.1}Cl$. To assess the structural distortions in $Li_2(OH)_{0.9}F_{0.1}Cl$ and in $Li_2OHF_{0.1}Cl_{0.9}$, the Li−Cl, Li−F, and Li−O radial distribution functions for $Li_2(OH)_{0.9}F_{0.1}Cl$ and $Li_2OHF_{0.1}Cl_{0.9}$ were calculated, see Figure S6. It is notable that the peaks in $Li_2OHF_{0.1}Cl_{0.9}$ have lower intensity and shift to the right more than that in $Li_2(OH)_{0.9}F_{0.1}Cl$. This suggests a weaker bonding between Li and anions in $Li_2OHF_{0.1}Cl_{0.9}$, and the greater distortions in $Li_2OHF_{0.1}Cl_{0.9}$ compared to $Li_2(OH)_{0.9}F_{0.1}Cl$.

In addition, as the OH reorientation time scale of $Li_2(OH)_{0.9}F_{0.1}Cl$ is shorter than that of Li_2OHCl, reducing the OH concentration, as suggested by Li et al.,[15] is not the only reason for the enhanced conductivity. Fluorination of an OH anionic sublattice of Li_2OHCl may also have caused local structural distortions that increased the OH orientation and the Li jumps. Most importantly, it is noted from Section 3.3 that E_{hull} of $Li_2(OH)_{0.9}F_{0.1}Cl$ and $Li_2OHF_{0.1}Cl_{0.9}$ is below 20 meV/atom. Therefore, the structural distortion that takes place for such a low level of F substitution does not affect the stability of the materials.[70] In conclusion, our analysis suggests the existence of an association among the local distortion of the lattice, the OH reorientation dynamics, and the increased bulk ionic conductivity in the protonated APs. Such distortion and associated OH dynamics could be further adjusted by tuning the doping level and the dopant type, e.g., Br or I. An in-depth study on this issue should be done in the future.

4. CONCLUSIONS

Using density functional theory and *ab initio* molecular dynamics simulations, several questions were answered regarding the impact of protonation and fluorination on the phase and electrochemical stabilities, elastic properties, and ionic conductivities of Li_2OHCl-based electrolytes. Li_2OHCl solid-state electrolyte (SSE), a protonated version of Li_3OCl, $Li_2(OH)_{0.9}F_{0.1}Cl$, a fluorinated variant of Li_2OHCl synthesized in 2016,[15] and $Li_2OHF_{0.1}Cl_{0.9}$, a novel material we proposed, were considered in this study. It is shown that Li_2OHCl, $Li_2(OH)_{0.9}F_{0.1}Cl$, and $Li_2OHF_{0.1}Cl_{0.9}$ are easier to synthesize than Li_3OCl, in agreement with the experimental literature.[14] Li_2OHCl, $Li_2(OH)_{0.9}F_{0.1}Cl$, and $Li_2OHF_{0.1}Cl_{0.9}$ are metastable at 0 K, but their energy above hull is below 20 meV/atom. This suggests that, in principle, an almost pure phase of the materials can be synthesized. The predicted electrochemical window of Li_2OHCl-based APs is ∼2.3 V vs Li/Li^+, in contrast to experimental reports that suggested values of 9 V vs Li/Li^+ as the electrochemical window of $Li_2(OH)_{0.9}F_{0.1}Cl$. It was found that, due to their higher concentration of Li vacancies, the elastic modulus of Li_2OHCl is much smaller than that of Li_3OCl. Interestingly, $Li_2OHF_{0.1}Cl_{0.9}$ has the highest ionic conductivity and lowest activation energy among the studied Li_2OHCl-based electrolytes. Such a high conductivity is attributed to the local structural distortions in the anionic sublattice brought by fluorination. Moreover, the reorientation characteristic time scales of the fluorinated electrolytes were found to be smaller than those in Li_2OHCl. The analysis suggests a correlation between the local structure distortion, increased OH reorientations, and bulk ionic conductivity.

■ ASSOCIATED CONTENT

Supporting Information

The Supporting Information is available free of charge at https://pubs.acs.org/doi/10.1021/acsami.0c17975.

Ground-state structures of the electrolytes; the estimation of elastic moduli from the computed elastic tensor; the analysis of the trajectories from the AIMD simulations; the decomposition reactions of the electrolytes with lithium metal; the Bader charge analysis; and the analysis of Li and OH trajectories (PDF)

https://dx.doi.org/10.1021/acsami.0c17975
ACS Appl. Mater. Interfaces 2020, 12, 55011−55022

AUTHOR INFORMATION

Corresponding Author

Francesco Ciucci − *Department of Mechanical and Aerospace Engineering and Department of Chemical and Biological Engineering, The Hong Kong University of Science and Technology, Hong Kong, China; Guangzhou HKUST Fok Ying Tung Research Institute, Guangzhou City 511458, China;* orcid.org/0000-0003-0614-5537; Email: francesco.ciucci@ust.hk

Authors

Mohammed B. Effat − *Department of Mechanical and Aerospace Engineering, The Hong Kong University of Science and Technology, Hong Kong, China*

Jiapeng Liu − *Department of Mechanical and Aerospace Engineering, The Hong Kong University of Science and Technology, Hong Kong, China;* orcid.org/0000-0001-8667-1929

Ziheng Lu − *Department of Mechanical and Aerospace Engineering, The Hong Kong University of Science and Technology, Hong Kong, China; Chinese Academy of Sciences, Shenzhen Institutes of Advanced Technology, Shenzhen 518055, China*

Ting Hei Wan − *Department of Mechanical and Aerospace Engineering, The Hong Kong University of Science and Technology, Hong Kong, China*

Antonino Curcio − *Department of Mechanical and Aerospace Engineering, The Hong Kong University of Science and Technology, Hong Kong, China*

Complete contact information is available at: https://pubs.acs.org/10.1021/acsami.0c17975

Funding

The authors would like to acknowledge the Research Grants Council of Hong Kong for the support through the projects (16207615, 16227016, and 16204517), the Guangzhou Science and Technology Program (No. 201807010074), and Hong Kong Innovation and Technology Fund (No. ITS/292/18FP).

Notes

The authors declare no competing financial interest.

ACKNOWLEDGMENTS

A.C. acknowledges the financial support from the Hong Kong Ph.D. Fellowship Scheme.

REFERENCES

(1) Tarascon, J. M.; Armand, M. Issues and Challenges Facing Rechargeable Lithium Batteries. *Nature* **2001**, *414*, 359−367.

(2) Zhang, Z.; Shao, Y.; Lotsch, B. V.; Hu, Y.-S.; Li, H.; Janek, J.; Nan, C.; Nazar, L.; Maier, J.; Armand, M. New Horizons for Inorganic Solid State Ion Conductors. *Energy Environ. Sci.* **2018**, *11*, 1945−1976.

(3) Effat, M. B.; Wu, C.; Ciucci, F. Modeling Efforts in the Key Areas of Thermal Management and Safety of Lithium Ion Battery Cells: A Mini Review. *Asia-Pac. J. Chem. Eng.* **2016**, *11*, 399−406.

(4) Arbizzani, C.; Gabrielli, G.; Mastragostino, M. Thermal Stability and Flammability of Electrolytes for Lithium-Ion Batteries. *J. Power Sources* **2011**, *196*, 4801−4805.

(5) Effat, M. B.; Lu, Z.; Belotti, A.; Yu, J.; Lyu, Y.-Q.; Ciucci, F. Towards Succinonitrile-Based Lithium Metal Batteries with Long Cycle Life: The Influence of Fluoroethylene Carbonate Loading and the Separator. *J. Power Sources* **2019**, *436*, No. 226802.

(6) Zhang, B.; Tan, R.; Yang, L.; Zheng, J.; Zhang, K.; Mo, S.; Lin, Z.; Pan, F. Mechanisms and Properties of Ion-Transport in Inorganic Solid Electrolytes. *Energy Storage Mater.* **2018**, *10*, 139−159.

(7) Zou, Z.; Li, Y.; Lu, Z.; Wang, D.; Cui, Y.; Guo, B.; Li, Y.; Liang, X.; Feng, J.; Li, H. Mobile Ions in Composite Solids. *Chem. Rev.* **2020**, *120*, 4169−4221.

(8) Zhao, Y.; Daemen, L. L. Superionic Conductivity in Lithium-Rich Anti-Perovskites. *J. Am. Chem. Soc.* **2012**, *134*, 15042−15047.

(9) Stegmaier, S.; Voss, J.; Reuter, K.; Luntz, A. C. Li+ Defects in a Solid-State Li Ion Battery: Theoretical Insights with a Li3ocl Electrolyte. *Chem. Mater.* **2017**, *29*, 4330−4340.

(10) Emly, A.; Kioupakis, E.; Van der Ven, A. Phase Stability and Transport Mechanisms in Antiperovskite Li3ocl and Li3obr Superionic Conductors. *Chem. Mater.* **2013**, *25*, 4663−4670.

(11) Dondelinger, M.; Swanson, J.; Nasymov, G.; Jahnke, C.; Qiao, Q.; Wu, J.; Widener, C.; Numan-Al-Mobin, A. M.; Smirnova, A. Electrochemical Stability of Lithium Halide Electrolyte with Antiperovskite Crystal Structure. *Electrochim. Acta* **2019**, *306*, 498−505.

(12) Dawson, J. A.; Attari, T. S.; Chen, H.; Emge, S. P.; Johnston, K. E.; Islam, M. S. Elucidating Lithium-Ion and Proton Dynamics in Anti-Perovskite Solid Electrolytes. *Energy Environ. Sci.* **2018**, *11*, 2993−3002.

(13) Song, A.-Y.; Xiao, Y.; Turcheniuk, K.; Upadhya, P.; Ramanujapuram, A.; Benson, J.; Magasinski, A.; Olguin, M.; Meda, L.; Borodin, O.; Yushin, G. Protons Enhance Conductivities in Lithium Halide Hydroxide/Lithium Oxyhalide Solid Electrolytes by Forming Rotating Hydroxy Groups. *Adv. Energy Mater.* **2017**, No. 1700971.

(14) Hanghofer, I.; Redhammer, G. nJ.; Rohde, S.; Hanzu, I.; Senyshyn, A.; Wilkening, H. M. R.; Rettenwander, D. Untangling the Structure and Dynamics of Lithium-Rich Anti-Perovskites Envisaged as Solid Electrolytes for Batteries. *Chem. Mater.* **2018**, *30*, 8134−8144.

(15) Li, Y.; Zhou, W.; Xin, S.; Li, S.; Zhu, J.; Lü, X.; Cui, Z.; Jia, Q.; Zhou, J.; Zhao, Y.; Goodenough, J. B. Fluorine-Doped Antiperovskite Electrolyte for All-Solid-State Lithium-Ion Batteries. *Angew. Chem., Int. Ed.* **2016**, *55*, 9965−9968.

(16) Wang, F.; Evans, H. A.; Kim, K.; Yin, L.; Li, Y.; Tsai, P.-C.; Liu, J.; Lapidus, S. H.; Brown, C. M.; Siegel, D. J.; Chiang, Y.-M. Dynamics of Hydroxyl Anions Promotes Lithium Ion Conduction in Antiperovskite Li2ohcl. *Chem. Mater.* **2020**, *32*, 8481−8491.

(17) Hood, Z. D.; Wang, H.; Samuthira Pandian, A.; Keum, J. K.; Liang, C. Li2ohcl Crystalline Electrolyte for Stable Metallic Lithium Anodes. *J. Am. Chem. Soc.* **2016**, *138*, 1768−1771.

(18) Schwering, G.; Hönnerscheid, A.; van Wüllen, L.; Jansen, M. High Lithium Ionic Conductivity in the Lithium Halide Hydrates $Li_{3-N}(Oh_n)Cl$ $(0.83 \leq N \leq 2)$ and $Li_{3-N}(Oh_n)Br$ $(1 \leq N \leq 2)$ at Ambient Temperatures. *ChemPhysChem* **2003**, *4*, 343−348.

(19) Song, A. Y.; Turcheniuk, K.; Leisen, J.; Xiao, Y.; Meda, L.; Borodin, O.; Yushin, G. Understanding Li-Ion Dynamics in Lithium Hydroxychloride (Li2ohcl) Solid State Electrolyte Via Addressing the Role of Protons. *Adv. Energy Mater.* **2020**, *10*, No. 1903480.

(20) Yin, L.; Yuan, H.; Kong, L.; Lu, Z.; Zhao, Y. Engineering Frenkel Defects of Anti-Perovskite Solid-State Electrolytes and Their Applications in All-Solid-State Lithium-Ion Batteries. *Chem. Commun.* **2020**, *56*, 1251−1254.

(21) McGrogan, F. P.; Swamy, T.; Bishop, S. R.; Eggleton, E.; Porz, L.; Chen, X.; Chiang, Y. M.; Van Vliet, K. J. Compliant yet Brittle Mechanical Behavior of Li2s−P2s5 Lithium-Ion-Conducting Solid Electrolyte. *Adv. Energy Mater.* **2017**, *7*, No. 1602011.

(22) Kresse, G.; Furthmüller, J. Efficient Iterative Schemes for Ab Initio Total-Energy Calculations Using a Plane-Wave Basis Set. *Phys. Rev. B* **1996**, *54*, 11169.

(23) Blöchl, P. E. Projector Augmented-Wave Method. *Phys. Rev. B* **1994**, *50*, 17953.

(24) Perdew, J. P.; Burke, K.; Ernzerhof, M. Generalized Gradient Approximation Made Simple. *Phys. Rev. Lett.* **1996**, *77*, 3865.

(25) Perdew, J. P.; Ruzsinszky, A.; Csonka, G. I.; Vydrov, O. A.; Scuseria, G. E.; Constantin, L. A.; Zhou, X.; Burke, K. Restoring the

Density-Gradient Expansion for Exchange in Solids and Surfaces. *Phys. Rev. Lett.* **2008**, *100*, No. 136406.
(26) Heyd, J.; Scuseria, G. E.; Ernzerhof, M. Hybrid Functionals Based on a Screened Coulomb Potential. *J. Chem. Phys.* **2003**, *118*, 8207−8215.
(27) Ong, S. P.; Richards, W. D.; Jain, A.; Hautier, G.; Kocher, M.; Cholia, S.; Gunter, D.; Chevrier, V. L.; Persson, K. A.; Ceder, G. Python Materials Genomics (Pymatgen): A Robust, Open-Source Python Library for Materials Analysis. *Comput. Mater. Sci.* **2013**, *68*, 314−319.
(28) Jain, A.; Ong, S. P.; Hautier, G.; Chen, W.; Richards, W. D.; Dacek, S.; Cholia, S.; Gunter, D.; Skinner, D.; Ceder, G.; Persson, K. A. Commentary: The Materials Project: A Materials Genome Approach to Accelerating Materials Innovation. *APL Mater.* **2013**, *1*, No. 011002.
(29) Jain, A.; Montoya, J.; Dwaraknath, S.; Zimmermann, N. E.; Dagdelen, J.; Horton, M.; Huck, P.; Winston, D.; Cholia, S.; Ong, S. P. The Materials Project: Accelerating Materials Design through Theory-Driven Data and Tools. In *Handbook of Materials Modeling*; Springer: Cham, 2018.
(30) de Jong, M.; Chen, W.; Angsten, T.; Jain, A.; Notestine, R.; Gamst, A.; Sluiter, M.; Krishna Ande, C.; van der Zwaag, S.; Plata, J. J.; Toher, C.; Curtarolo, S.; Ceder, G.; Persson, K. A.; Asta, M. Charting the Complete Elastic Properties of Inorganic Crystalline Compounds. *Sci. Data* **2015**, *2*, No. 150009.
(31) Ong, S. P.; Wang, L.; Kang, B.; Ceder, G. Li−Fe−P−O2 Phase Diagram from First Principles Calculations. *Chem. Mater.* **2008**, *20*, 1798−1807.
(32) Deng, Z.; Zhu, Z.; Chu, I.-H.; Ong, S. P. Data-Driven First-Principles Methods for the Study and Design of Alkali Superionic Conductors. *Chem. Mater.* **2016**, *29*, 281−288.
(33) Urban, A.; Seo, D.-H.; Ceder, G. Computational Understanding of Li-Ion Batteries. *npj Comput. Mater.* **2016**, *2*, 16002.
(34) Peljo, P.; Girault, H. H. Electrochemical Potential Window of Battery Electrolytes: The Homo−Lumo Misconception. *Energy Environ. Sci.* **2018**, *11*, 2306−2309.
(35) Tang, H.; Deng, Z.; Lin, Z.; Wang, Z.; Chu, I.-H.; Chen, C.; Zhu, Z.; Zheng, C.; Ong, S. P. Probing Solid−Solid Interfacial Reactions in All-Solid-State Sodium-Ion Batteries with First-Principles Calculations. *Chem. Mater.* **2017**, *30*, 163−173.
(36) Deng, Z.; Wang, Z.; Chu, I.-H.; Luo, J.; Ong, S. P. Elastic Properties of Alkali Superionic Conductor Electrolytes from First Principles Calculations. *J. Electrochem. Soc.* **2016**, *163*, A67−A74.
(37) Lee, J. G. *Computational Materials Science: An Introduction*; CRC Press, 2016.
(38) Mehrer, H. *Diffusion in Solids: Fundamentals, Methods, Materials, Diffusion-Controlled Processes*; Springer Science & Business Media, 2007; Vol. *155*.
(39) Compaan, K.; Haven, Y. Correlation Factors for Diffusion in Solids. *Trans. Faraday Soc.* **1956**, *52*, 786−801.
(40) Rasmussen, C. Advanced Lectures on Machine Learning. *Lect. Notes Comput. Sci.* **2004**, *3176*, 63−71.
(41) Liu, J.; Lu, Z.; Effat, M. B.; Ciucci, F. A Theoretical Study on the Stability and Ionic Conductivity of the Na11m2ps12 (M = Sn, Ge) Superionic Conductors. *J. Power Sources* **2019**, *409*, 94−101.
(42) Humphrey, W.; Dalke, A.; Schulten, K. Vmd: Visual Molecular Dynamics. *J. Mol. Graphics* **1996**, *14*, 33−38.
(43) Howard, J.; Hood, Z. D.; Holzwarth, N. A. W. Fundamental Aspects of the Structural and Electrolyte Properties of Li2ohcl from Simulations and Experiment. *Phys. Rev. Mater.* **2017**, *1*, No. 075406.
(44) Sun, W.; Dacek, S. T.; Ong, S. P.; Hautier, G.; Jain, A.; Richards, W. D.; Gamst, A. C.; Persson, K. A.; Ceder, G. The Thermodynamic Scale of Inorganic Crystalline Metastability. *Sci. Adv.* **2016**, *2*, No. e1600225.
(45) Yim, C.-H.; Abu-Lebdeh, Y. A. Connection between Phase Diagram, Structure and Ion Transport in Liquid, Aqueous Electrolyte Solutions of Lithium Chloride. *J. Electrochem. Soc.* **2018**, *165*, A547−A556.
(46) Emery, A. A.; Wolverton, C. High-Throughput Dft Calculations of Formation Energy, Stability and Oxygen Vacancy Formation Energy of Abo3 Perovskites. *Sci. Data* **2017**, *4*, No. 170153.
(47) Kamphaus, E. P.; Angarita-Gomez, S.; Qin, X.; Shao, M.; Balbuena, P. B. Effects of Solid Electrolyte Interphase Components on the Reduction of Lifsi over Lithium Metal. *ChemPhysChem* **2020**, *21*, 1310−1317.
(48) Tu, Z.; Choudhury, S.; Zachman, M. J.; Wei, S.; Zhang, K.; Kourkoutis, L. F.; Archer, L. A. Designing Artificial Solid-Electrolyte Interphases for Single-Ion and High-Efficiency Transport in Batteries. *Joule* **2017**, *1*, 394−406.
(49) Li, S.; Zhu, J.; Wang, Y.; Howard, J. W.; Lü, X.; Li, Y.; Kumar, R. S.; Wang, L.; Daemen, L. L.; Zhao, Y. Reaction Mechanism Studies Towards Effective Fabrication of Lithium-Rich Anti-Perovskites Li3OX (X = Cl, Br). *Solid State Ionics* **2016**, *284*, 14−19.
(50) Zhu, Y.; He, X.; Mo, Y. Origin of Outstanding Stability in the Lithium Solid Electrolyte Materials: Insights from Thermodynamic Analyses Based on First-Principles Calculations. *ACS Appl. Mater. Interfaces* **2015**, *7*, 23685−23693.
(51) Sivey, J. D.; Roberts, A. L. Assessing the Reactivity of Free Chlorine Constituents Cl2, Cl2o, and Hocl toward Aromatic Ethers. *Environ. Sci. Technol.* **2012**, *46*, 2141−2147.
(52) Zhang, Y.; Zhao, Y.; Chen, C. Ab Initio Study of the Stabilities of and Mechanism of Superionic Transport in Lithium-Rich Antiperovskites. *Phys. Rev. B* **2013**, *87*, No. 134303.
(53) Xiao, Y.; Miara, L. J.; Wang, Y.; Ceder, G. Computational Screening of Cathode Coatings for Solid-State Batteries. *Joule* **2019**, *3*, 1252−1275.
(54) Zhang, X.-Q.; Cheng, X.-B.; Chen, X.; Yan, C.; Zhang, Q. Fluoroethylene Carbonate Additives to Render Uniform Li Deposits in Lithium Metal Batteries. *Adv. Funct. Mater.* **2017**, *27*, No. 1605989.
(55) Xiao, Y.; Wang, Y.; Bo, S.-H.; Kim, J. C.; Miara, L. J.; Ceder, G. Understanding Interface Stability in Solid-State Batteries. *Nat. Rev. Mater.* **2019**, 1−22.
(56) Swamy, T.; Chen, X.; Chiang, Y.-M. Electrochemical Redox Behavior of Li Ion Conducting Sulfide Solid Electrolytes. *Chem. Mater.* **2019**, *31*, 707−713.
(57) Schwietert, T. K.; Arszelewska, V. A.; Wang, C.; Yu, C.; Vasileiadis, A.; de Klerk, N. J. J.; Hageman, J.; Hupfer, T.; Kerkamm, I.; Xu, Y.; van der Maas, E.; Kelder, E. M.; Ganapathy, S.; Wagemaker, M. Clarifying the Relationship between Redox Activity and Electrochemical Stability in Solid Electrolytes. *Nat. Mater.* **2020**, *19*, 428−435.
(58) Zhang, W.; Richter, F. H.; Culver, S. P.; Leichtweiss, T.; Lozano, J. G.; Dietrich, C.; Bruce, P. G.; Zeier, W. G.; Janek, J. r. Degradation Mechanisms at the Li10gep2s12/Licoo2 Cathode Interface in an All-Solid-State Lithium-Ion Battery. *ACS Appl. Mater. Interfaces* **2018**, *10*, 22226−22236.
(59) Tian, H.-K.; Qi, Y. Simulation of the Effect of Contact Area Loss in All-Solid-State Li-Ion Batteries. *J. Electrochem. Soc.* **2017**, *164*, E3512−E3521.
(60) Wan, T. H.; Ciucci, F. Electro-Chemo-Mechanical Modeling of Solid-State Batteries. *Electrochim. Acta* **2020**, *331*, No. 135355.
(61) Sakuda, A.; Hayashi, A.; Tatsumisago, M. Sulfide Solid Electrolyte with Favorable Mechanical Property for All-Solid-State Lithium Battery. *Sci. Rep.* **2013**, *3*, No. 2261.
(62) Shin, B. R.; Nam, Y. J.; Kim, J. W.; Lee, Y.-G.; Jung, Y. S. Interfacial Architecture for Extra Li+ Storage in All-Solid-State Lithium Batteries. *Sci. Rep.* **2014**, *4*, No. 5572.
(63) Schnell, J.; Günther, T.; Knoche, T.; Vieider, C.; Köhler, L.; Just, A.; Keller, M.; Passerini, S.; Reinhart, G. All-Solid-State Lithium-Ion and Lithium Metal Batteries—Paving the Way to Large-Scale Production. *J. Power Sources* **2018**, *382*, 160−175.
(64) Qi, Y.; Hector, L. G.; James, C.; Kim, K. J. Lithium Concentration Dependent Elastic Properties of Battery Electrode Materials from First Principles Calculations. *J. Electrochem. Soc.* **2014**, *161*, F3010−F3018.
(65) Yu, S.; Schmidt, R. D.; Garcia-Mendez, R.; Herbert, E.; Dudney, N. J.; Wolfenstine, J. B.; Sakamoto, J.; Siegel, D. J. Elastic

https://dx.doi.org/10.1021/acsami.0c17975
ACS Appl. Mater. Interfaces 2020, 12, 55011−55022

Properties of the Solid Electrolyte Li7la3zr2o12 (Llzo). *Chem. Mater.* **2016**, *28*, 197−206.
(66) Bader, R. F. Atoms in Molecules. In *Encyclopedia of Computational Chemistry*; Wiley Online Library, 1990.
(67) Seabold, S.; Perktold, J. In *Statsmodels: Econometric and Statistical Modeling with Python*, Proceedings of the 9th Python in Science Conference, 2010; p 61.
(68) Laage, D.; Stirnemann, G.; Sterpone, F.; Rey, R.; Hynes, J. T. Reorientation and Allied Dynamics in Water and Aqueous Solutions. *Annu. Rev. Phys. Chem.* **2011**, *62*, 395−416.
(69) Shannon, R. D. Revised Effective Ionic Radii and Systematic Studies of Interatomic Distances in Halides and Chalcogenides. *Acta Crystallogr., Sect. A: Cryst. Phys., Diffr., Theor. Gen. Crystallogr.* **1976**, *32*, 751−767.
(70) Kim, K.; Siegel, D. J. Correlating Lattice Distortions, Ion Migration Barriers, and Stability in Solid Electrolytes. *J. Mater. Chem. A* **2019**, *7*, 3216−3227.

https://dx.doi.org/10.1021/acsami.0c17975
ACS Appl. Mater. Interfaces 2020, 12, 55011−55022